

Unmanned Aerial Vehicle Mediated Drug Delivery for First Aid

Tao Sheng, Rui Jin, Changwei Yang, Ke Qiu, Mingyang Wang, Jiaqi Shi, Jingyu Zhang, Yuman Gao, Qing Wu, Xin Zhou, Hao Wang, Juan Zhang, Qin Fang, Neng Pan, Yanan Xue, Yue Wang, Rong Xiong, Fei Gao, Yuqi Zhang, Haojian Lu,* Jicheng Yu,* and Zhen Gu*

Acknowledgements Page 9

T.S. and R.J. contributed equally to this work.

Timely administration of key medications toward patients with sudden diseases is critical to saving lives. However, slow transport of first-aid therapeutics and the potential absence of trained people for drug usage can lead to severe injuries or even death. Herein, an unmanned aerial vehicle (UAV)-mediated first-aid system for targeted delivery (*uFAST*) is developed. It allows unattended administration of emergency therapeutics-loaded transdermal microneedle (MN) patches toward patients to relieve symptoms by a contact-triggered microneedle applicator (CTMA). The implementability and safety of the *uFAST* for first aid is demonstrated in a severe hypoglycemic pig model by automatically delivering a glucagon patch with immediate and bioresponsive dual release modes. This platform technique may facilitate the development of UAV-mediated first-aid treatments for other sudden diseases.

1. Introduction

First aid is crucial for patients with sudden illnesses, such as myocardial infarction, severe hypoglycemia, and stroke.^[1] In these situations, the patients may face an extreme risk of death if treatment is not provided promptly; thus, time is life in these cases.^[2] However, there are still a large number of deaths worldwide caused by a lack of timely resuscitation, which results from the shortage of emergency equipment around the patient, the inability of the patient to call for help, or traffic congestion.^[3] Moreover, drug-based first aid is mainly dependent on intravenous or subcutaneous injection of

T. Sheng, C. Yang, J. Shi, Q. Wu, H. Wang, J. Zhang, Y. Zhang, J. Yu, Z. Gu
Key Laboratory of Advanced Drug Delivery Systems of Zhejiang Province
College of Pharmaceutical Sciences

Zhejiang University
Hangzhou 310058, China
E-mail: yujicheng@zju.edu.cn; guzhen@zju.edu.cn

R. Jin, K. Qiu, M. Wang, J. Zhang, Y. Gao, X. Zhou, Q. Fang, N. Pan,
Y. Xue, Y. Wang, R. Xiong, F. Gao, H. Lu
State Key Laboratory of Industrial Control and Technology
Zhejiang University
Hangzhou 310027, China
E-mail: luhaojian@zju.edu.cn

R. Jin, K. Qiu, M. Wang, J. Zhang, Y. Gao, X. Zhou, Q. Fang, N. Pan,
Y. Xue, Y. Wang, R. Xiong, F. Gao, H. Lu
Institute of Cyber-Systems and Control
the Department of Control Science and Engineering
Zhejiang University
Hangzhou 310027, China

R. Jin, M. Wang, Y. Gao, X. Zhou, N. Pan, F. Gao
Huzhou Institute of Zhejiang University
Huzhou 313000, China

Y. Zhang
Department of Burns and Wound Center
Second Affiliated Hospital
School of Medicine
Zhejiang University
Hangzhou 310009, China

H. Lu
Stomatology Hospital, School of Stomatology
Zhejiang University School of Medicine
Clinical Reach Center for Oral Disease of Zhejiang Province
Key Laboratory of Oral Biomedical Research of Zhejiang Province
Cancer Center of Zhejiang University
Hangzhou 310006, China

J. Yu, Z. Gu
Liangzhu Laboratory
Zhejiang University Medical Center
Hangzhou 311121, China

J. Yu, Z. Gu
Department of General Surgery
Sir Run Run Shaw Hospital
School of Medicine
Zhejiang University
Hangzhou 310016, China

J. Yu, Z. Gu
Jinhua Institute of Zhejiang University
Jinhua 321299, China

Z. Gu
MOE Key Laboratory of Macromolecular Synthesis
and Functionalization
Department of Polymer Science
Zhejiang University
Hangzhou 310027, China

 The ORCID identification number(s) for the author(s) of this article
can be found under <https://doi.org/10.1002/adma.202208648>.

DOI: 10.1002/adma.202208648

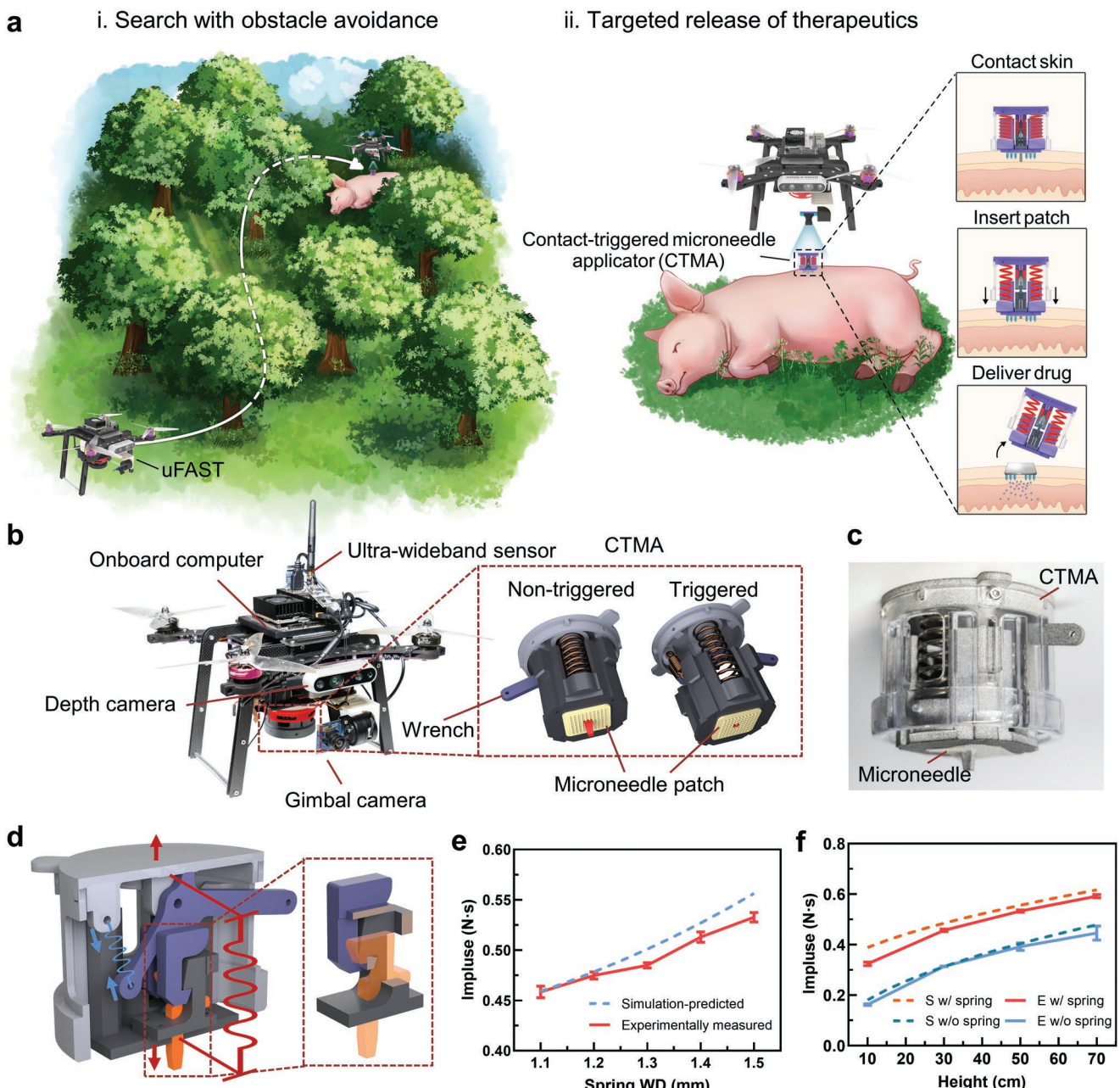


Figure 1. Schematic and characterization of UAV-mediated first-aid system for targeted drug delivery (uFAST). a) Schematic of uFAST. Once the UAV receives the emergency signal, it takes off immediately and reaches the patient to release the CTMA, which subsequently autonomously administers the MN patch into the skin for targeted drug delivery. b) Schematic of the components of the uFAST, including a UAV, a CTMA, and an MN patch. The MN patch is fixed onto the CTMA, which is secured in the UAV. c) Physical diagram of the CTMA and MN patch. d) Schematic of the CTMA. When the CTMA is untriggered, the pre-compressed spring (red) pushes the slidable base (black), and the tension spring (blue) pulls the bridge (purple) that is locked by the trigger (orange) and prevents the base from sliding out. Once the trigger touches the skin surface, it rises up to unlock the bridge, and the base is ejected out by the compressed spring. e) Simulation-predicted (dashed line) and experimentally measured (solid line) impulse of the CTMA with different spring wire diameters (WD) at RH of 0.5 m ($n = 4$). f) Simulation-predicted (S, dashed line) and experimentally measured (E, solid line) impulse of the CTMA with and without spring (1.5 mm WD) at RH from 0.1 m to 0.7 m ($n = 4$). In (e,f), data are presented as mean \pm standard deviation (s.d.).

emergency drugs, while this process always needs to be operated by professionals. In addition, inappropriate administration of the syringe needles for injections by patients may cause secondary injury, such as the risk of residual needle fracture in the skin, infection, as well as inflammation.^[4]

Herein, we describe an unmanned aerial vehicle (UAV)-mediated first-aid system for targeted delivery (uFAST) that can achieve autonomous administration of emergency medication without the involvement of additional or conscious persons (Figure 1a). The UAV can be initiated by an emergency signal

with the positioning information from the patients, and it is able to reach the vicinity of the positioning signal based on an online calculated trajectory with real-time obstacle avoidance capability. In this system, we utilize a microneedle (MN) patch as an emergency device because MNs can provide convenient, safe, and efficient administration. Such transdermal formats can be tailored to achieve rapid drug release from a dissolvable tip as well as bioresponsive controlled release from a crosslinked matrix.^[5] Of note, in order to adapt the MN patch to the UAV and realize UAV-mediated drug administration, a contact-triggered microneedle applicator (CTMA) is designed to provide a sufficient force to insert MNs upon contact with the skin (Figure 1b,c). When the UAV searches and identifies the patient, it hovers at a proper height and subsequently releases the CTMA to apply the drug-loaded MNs into the skin for emergency care.

We further demonstrate the implementability and safety of the uFAST for first aid in a severe hypoglycemia disease model. Hypoglycemia is a common side effect occurring in people with diabetes receiving insulin treatment, and severe hypoglycemia may lead to coma, brain damage, or even death.^[6] As severe hypoglycemia often leads to sudden fainting or occurs while sleeping at night,^[7] the continuous glucose monitoring system (CGMS) on diabetic people that is able to real-time alert hypoglycemia could serve as the danger signal source to pair the uFAST for timely administration of the glucose-elevating drug (glucagon).^[8] In order to ensure accurate dosing of glucagon, a dual-mode microneedle patch (DM-MN) is developed to realize an immediate release of a basal dose as well as a sustained glucose-dependent release of a subsequent dose. In an insulin-overdosing hypoglycemic diabetic minipig model, we further substantiate that the uFAST integrated with DM-MN could facilitate a timely aid in minutes, to alleviate the risk of severe hypoglycemia.

2. Results

2.1. Design and Characterization of the Autonomous Drug Delivery System

The autonomous drug delivery system consists of the CTMA, the release unit, the gimbal camera unit, and the base platform attached to the bottom of the UAV. The detailed delivery gear design for the UAV is shown in Figure 1b. We equipped the release unit for locating the CTMA (Figure S1, Supporting Information), the onboard ultra-wideband (UWB) sensor for measuring the relative distance to correct the position of the patient, and the gimbal camera for identifying the patient to obtain the releasing point. The core part of the drug delivery module is the CTMA which administers the therapeutics into the body via a MN array patch (Figure 1c). The CTMA was designed and built to be lightweight (75 g), reducing the payload during flight to increase the first-aid distance. Meanwhile, due to the necessity of the powerful force in MN patch application, a contact-triggered system was designed to release the pre-stored energy. The CTMA is mainly composed of trigger elements, energy storage elements, and a MN patch. The schematic diagram of the CTMA is shown in Figure 1d and

Figure S2, Supporting Information. When the trigger at the bottom of CTMA touches the skin surface, the springs can release sufficient energy to eject the slidible base so that the MN patch attached can be inserted into the skin. After completing the first-aid task, the CTMA can be readily reused by pulling back the wrench.

Considering the administration mode of the MN patch, sufficient pressure lasting for a period of time is essential for successful penetration. To this end, we evaluated the insertion performance of the CTMA by the integral of force with time (impulse). The impulse

I generated by the CTMA was calculated as $I = mv_1 - mv_0$, where m was the mass of the CTMA, and v_0 and v_1 were the velocities of the CTMA before and after applying respectively.

The simulation (see details in the Experimental Section; Equation (S1) and Figure S3, Supporting Information) predicted that the CTMA with the thicker springs or released from a higher position could generate a greater impulse (Figure 1e,f).^[9] Real-world experiments were further conducted to validate the hypothesis (Figure 1e,f; Videos S1 and S2, Supporting Information). The high-speed camera was used to measure the velocity of the CTMA (Figure S4, Supporting Information). As it was difficult to reset the CTMA when wire diameter (WD) > 1.5 mm, the springs of 1.5 mm WD were selected in the following study to evaluate the performance of CTMA at different release heights (RHs).

In the final process of identification, the height of the uFAST determines the accuracy of the operating localization position. Due to the ground effect, the uFAST cannot hover stably at a relatively low position. Considering the magnitude of generated impulse, an optimized RH value of 50 cm was selected in the following experiments.

2.2. Combination of CTMA and Microneedle Patch

The MN patch was immobilized on the CTMA through frictional force by cutting a pinhole in the MN patch slightly larger than the bottom area of the trigger element. Taking advantage of the pressure-sensitive films, the MN patches implementation comparison on the minipig skin between manually pressing and CTMA could be revealed directly, indicating the pressure generated by CTMA was uniform compared to that generated manually (Figure 2a). In addition, the hematoxylin and eosin (H&E)-stained section image further validated the insertion of the MNs into the minipig skin by CTMA (Figure 2b).

Furthermore, the MN insertion process was captured under high-speed photography (Figure 2c; Video S3, Supporting Information). The slow-motion video of the MN insertion process exhibited three main stages, that is, descending, triggering, and inserting. In Figure 2d and Video S4, Supporting Information, the device fixed by glue (springs were invalid) was tested under the same experimental conditions but could hardly insert the MNs. With the aid of the high-speed camera, it could be perceived that the base corner touched the skin first in most cases, resulting in the putting straight of CTMA. After that, the springs could eject the base out during pose adjusting and provide sufficient force to deform the skin to fit the MN patch (Figure 2e).

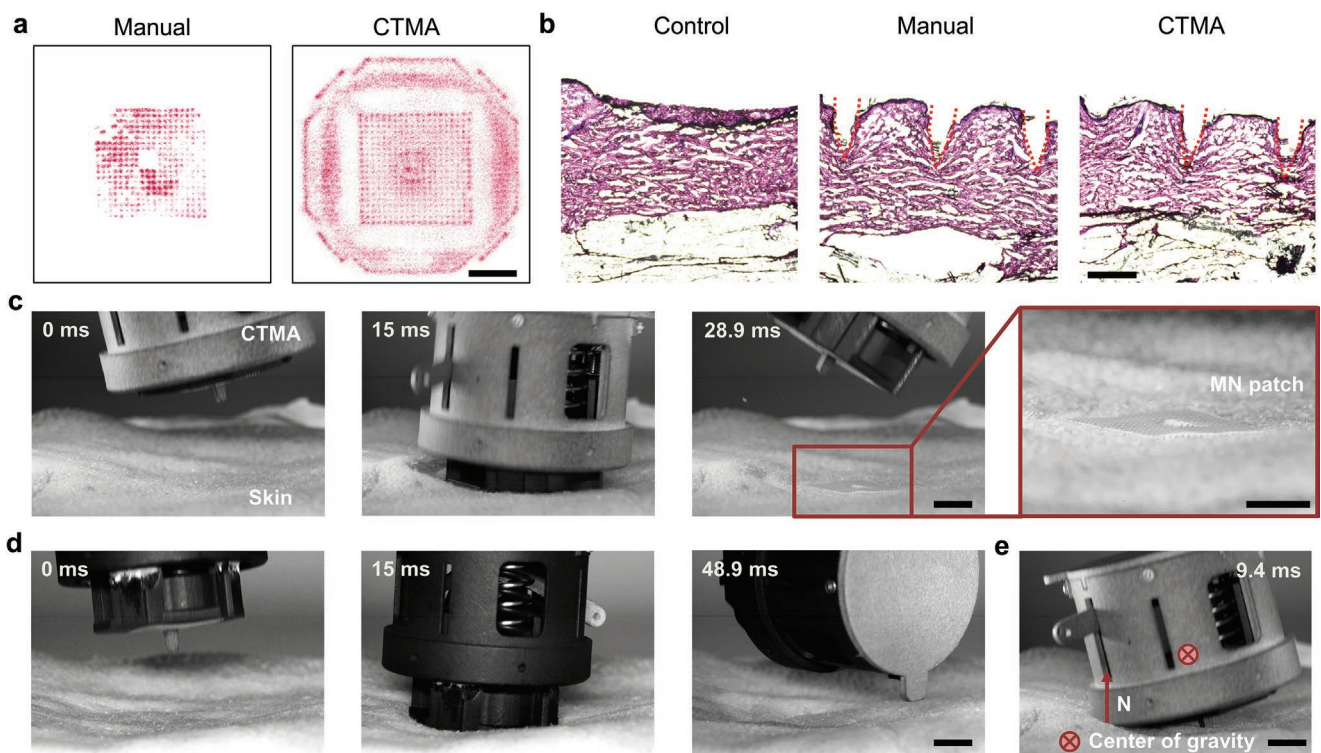


Figure 2. Combined administration of the CTMA and MN patch. a) Visualization of the contact force by the pressure-sensitive films. Scale bar: 1 cm. b) Representative hematoxylin and eosin (H&E) stained sections of MNs penetrating into the minipig skin by different methods (manually and CTMA). Scale bar: 500 μ m. c,d) The process of the MN patch administration by the CTMA with spring (c) and without spring (d) through the high-speed photography (imaging at 1800 frames per s). Scale bar: 1.2 cm. e) Representative force diagram of the CTMA with spring when it touched the skin surface. Scale bar: 1.2 cm.

As the RHs may influence the CTMA drop position, we tested the positioning accuracy of CTMA-delivered MN patch both in vitro and in vivo. It demonstrated that the MN patch drop position was moved away from the release position as the RH was increased (Figure S5A,B, Supporting Information). With the RH of 50 cm, the average releasing position error (distance from the release position to the center of the MN path drop position) could be controlled within 2.44 cm in vitro (Figure S5A, Supporting Information) and 4.6 cm in vivo (Figure S5C,D, Supporting Information), respectively. The minimum circle area encompassing all MN patch positions was considered as the minimal dimension, which could be controlled in a circle with a radius of 4.31 cm in vitro (Figure S5A, Supporting Information) and 9.22 cm in vivo (Figure S5D, Supporting Information). These results suggested that precise and area targeted drug delivery with the MN patch could be achieved by CTMA.

2.3. Preparation and Characterization of the Glucagon-Loaded DM-MN Patch

Glucagon is available as an emergency medication to treat severe hypoglycemia by stimulating the breakdown of liver glycogen to increase blood glucose levels.^[10] In order to prevent an overdose of glucagon, a DM-MN patch with a bilayer structure was developed. The DM-MN was comprised of two action

modules: the MN tip made by the water-soluble polymer could immediately release glucagon to rapidly raise the blood glucose once inserted into the skin; the MN body made by glucose-responsive polymeric matrix could sustainably provide additional glucagon subsequently in a glucose-dependent manner to achieve better blood glucose regulation and prevent the blood glucose becoming too high or staying too low. The DM-MN patch was prepared by a two-step fabrication method based on two types of silicone MN molds. The immediate release module of DM-MN was first prepared from a mixture of glucagon (GC) and N-vinylpyrrolidone (NVP) by the in situ photopolymerization at 4 °C, and the glucose-responsive release module was subsequently fabricated from the mixture of the glucagon analog (GA), NVP, ethylene glycol dimethacrylate (EGDMA), (4-((2-acrylamidoethyl) carbamoyl)-3-fluorophenyl) boronic acid (3FPBA), and 2-(dimethylamino) ethyl acrylate (DMAEA) by the same method (Figure 3a,b; Figure S6, Supporting Information).

The prepared DM-MN patch was made up of a 20 × 20 array of microstructures with a central spacing of 800 μ m between the adjacent needles. The base width and height of the needle tip arrays were 400 and 500 μ m, and the base width and height of the needle body array were 400 and 400 μ m, respectively (Figure S6, Supporting Information). The fluorescence microscopy images of the DM-MN revealed the bilayer structure of the fluorescein isothiocyanate (FITC)-labeled GC loaded needle tip and the rhodamine-B-labelled GA loaded needle body (Figure 3c). The successful assembling of the two modules

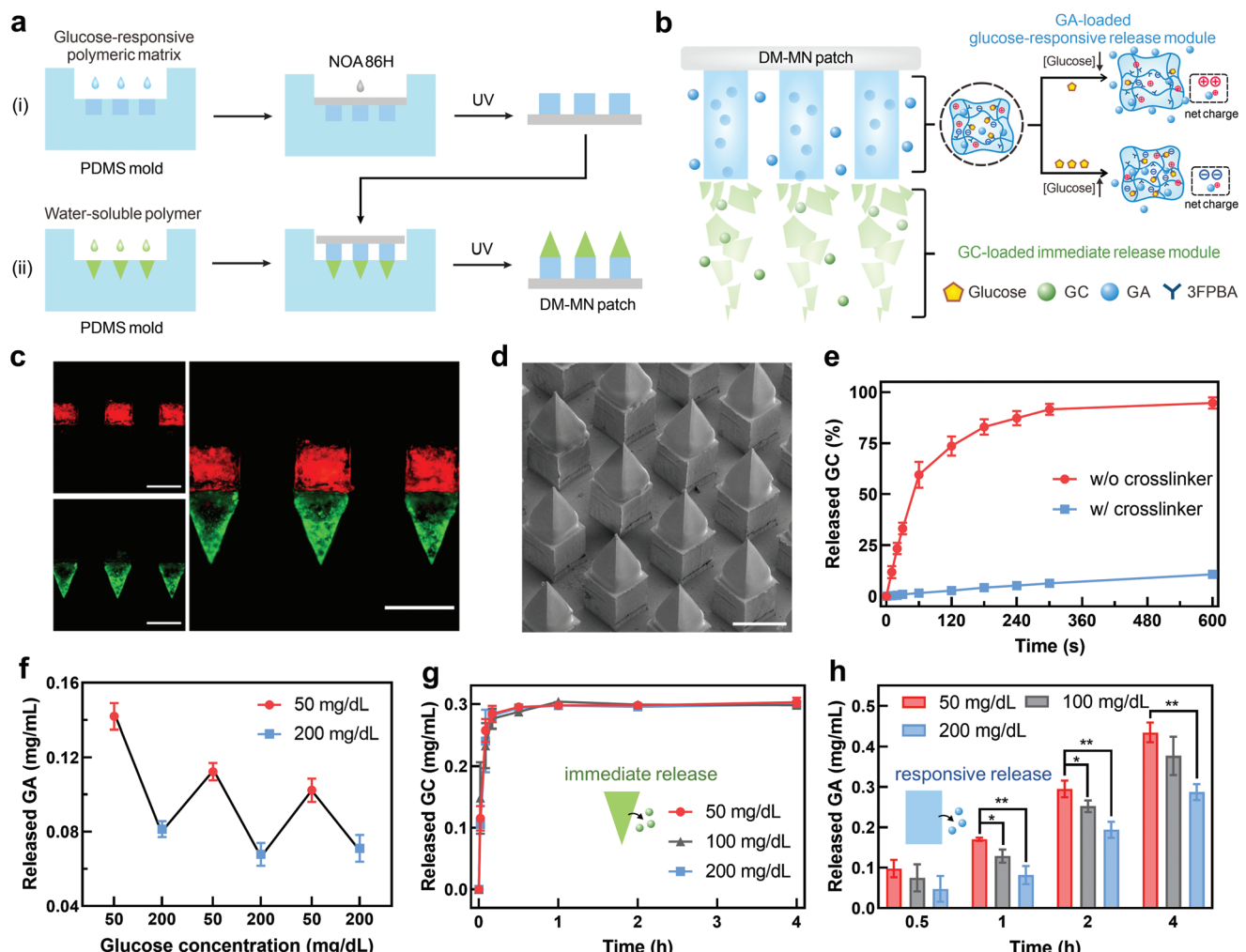


Figure 3. Characterization of the glucagon-loaded DM-MN patch. a) Schematic of the fabrication process of a DM-MN patch from silicone molds using an in situ photopolymerization method. b) Mechanism of immediate GC release and GA glucose-responsive release from DM-MNs. c) Representative fluorescence microscopy images of the DM-MN patch containing the immediate release module (FITC-GC) and glucose-responsive release module (Rhodamine B-GA). Scale bar: 500 μ m. d) Representative scanning electron microscopy images of the DM-MN patch. Scale bar: 500 μ m. e) In vitro accumulated release of GC from the immediate release polymeric matrix with (w/) and without (w/o) the crosslinker of EGDMA in PBS at 37 °C ($n = 3$). f) Pulsatile release pattern of GA by incubating in solution with different glucose concentrations of 50 and 200 mg dL⁻¹ alternately. Each incubation time is 20 min. g,h) In vitro accumulated release of GC (g) and GA (h) from the DM-MNs in varying glucose concentrations at 37 °C, pH 7.4 ($n = 3$). In (e-h), data are presented as mean \pm s.d. Statistical significance was determined by a two-tailed Student's *t* test. **P* < 0.05, ***P* < 0.01.

was further confirmed by scanning electron microscopy (SEM) images (Figure 3d), whereby the two modules were tightly connected (Figure S7, Supporting Information). In addition, the fracture force of the DM-MN was determined as 0.307 ± 0.013 N per needle by a tensile compression machine (Figure S8, Supporting Information), which was sufficient to penetrate the skin.^[5g,h]

To achieve immediate release of GC for hypoglycemic emergencies, the MN tip was fabricated by the polymerization of NVP without the crosslinker. As shown in Figure 3e, more than 75% of GC could be released in ≈ 2 min, while less than 20% of GC was released even in 10 min from the polymeric matrix crosslinked by EGDMA. Phenylboronic acid was selected as the glucose-sensitive unit in the glucose-responsive release module. It could reversibly interact with glucose to form negatively charged cyclic boronic esters under hyperglycemic conditions,

while dissociating to the uncharged group under hypoglycemic conditions, which led to an increased positive net charge within the MN polymeric matrix due to the presence of amino groups in DMAEA units (Figure 3b). As the isoelectric point (pI) of natural glucagon is ≈ 7.1 ,^[11] it has weak electrostatic interaction with the charge-switchable MN matrix in a physiological environment (pH 7.4). Therefore, a positively charged glucagon analog was synthesized by introducing two basic amino acids, arginine, to the C-terminus of glucagon. The resulting GA had an isoelectric point of ≈ 9.3 (Figure S9, Supporting Information). In vivo studies revealed that GA had a similar glucose-raising capacity compared to native glucagon (Figure S10, Supporting Information). In the glucose-responsive release module with a 1:0.8 ratio of 3FPBA to DMAEA, GA could be quickly released due to the electrostatic repulsion by the positively charged MN matrix under hypoglycemia, while the release rate slowed down

once returned to normoglycemia (Figure 3f; Figure S11, Supporting Information).

The dual-mode release behavior of DM-MN patches was further assessed in solutions with varying concentrations of glucose. As shown in Figure 3g,h, the resultant DM-MN patches could realize a rapid release of glucagon and a sustained glucose-dependent release of GA. In addition, the activity of the released GC and GA was similar to freshly dissolved native GC and GA in healthy mice (Figure S10, Supporting Information) because no additional extra organic solvent and the elevated temperature were involved during the fabrication process. The matrix-assisted laser desorption/ionization time-of-flight mass spectrum (MALDI-TOF-MS) analysis further confirmed that the released GC and GA remained intact throughout the polymerization process (Figure S12, Supporting Information). Moreover, the immediate release module showed insignificant toxicity at the various concentrations studied (Figure S13, Supporting Information), and the glucose-responsive release module that was not dissolvable in vivo could be intactly removed from the skin.

2.4. In Vivo Studies of DM-MN Integrated uFAST in the Hypoglycemic Diabetic Pig Model

We further assessed the performance of the uFAST in an insulin-overdosing hypoglycemic diabetic minipig model regarding the minipig skin structure being similar to human skin.^[12] Acute severe hypoglycemia in the streptozotocin-induced type 1 diabetic minipig was developed by subcutaneous overdosing of insulin (0.035 mg kg^{-1}). To achieve real-time and continuous recording of glucose levels in minipigs, a continuous glucose monitoring system (CGMS) was affixed to the inside of the hind legs of the minipigs. When hypoglycemia occurred, the CGMS could alert and generate a danger signal to be transmitted to the uFAST. In this study, a manual signal containing the coordinate information was sent to the uFAST when the minipig got hypoglycemia. We used a visual-inertial system (VINS), a robust visual-inertial odometry (VIO) framework, to localize the UAV,^[13] and a newly developed trajectory representation named minimum control (MINCO) for trajectory planning.^[14] Once the signal was sensed, the UAV took off equipped with the DM-MN patch. According to the target location signal and the obstacle map built from the real world, the UAV (FAST 330) could achieve automatic trajectory planning with obstacle avoidance capability.^[15] Meanwhile, the destination was corrected online by relocating the signal source through onboard UWB sensors (Equation (S2) and Figure S14, Supporting Information). When the UAV reached the source of the signal, the UAV could accurately hover over the minipig through auto-identification based on the pre-trained YOLOv5 neural network. Then, the UAV fell to 50 cm above the center of the minipig, and released the CTMA to achieve DM-MN application into the skin of the minipig (Figure 4a; Video S5, Supporting Information). As shown in Figure 4b, the DM-MN effectively penetrated the skin of the minipig by uFAST.

Following the application of the DM-MN patch via uFAST, the blood glucose of the hypoglycemic minipig rapidly returned

to the normoglycemic range within 90 min, which was similar to the groups that received DM-MN patches by pressing manually (Figure 4c). However, the minipigs without any treatment remained in the hypoglycemic state for more than 6 h (Figure S15, Supporting Information). Through comparing the different first-aid manners, the DM-MN integrated uFAST was able to achieve a fast glucose-raising effect as well as the manual pressing method, significantly minimizing the duration of hypoglycemia and reducing the risk of fatal danger (Figure 4d).

We further examined the plasma concentrations of GC and GA in the minipigs. As shown in Figure 4e,f, the DM-MN patches administered by either uFAST or manual pressing could achieve a similar rapid release of GC and the responsive release of GA (Figure S16, Supporting Information). GC released from the immediate release module reached the maximum blood concentration in 30 min, while GA from the glucose-responsive module reached the maximum blood concentration in 45–60 min, and the release rate of GA gradually decreased with the rise of blood glucose. We also monitored the change of the glucose levels in the blood using both the CGMS and glucometer, and found that blood glucose could reach the normal blood glucose range ≈60 min after the use of DM-MN, indicating a corresponding dependence on the concentration of GC and GA in plasma. The time for CGMS to detect the rise of blood glucose to the normal range was ≈90 minutes (Figure S17, Supporting Information), which may be related to the existence of lag in the detection of blood glucose by CGMS.^[16] Insignificant neutrophil infiltration and inflammatory response were noted after treatment with the DM-MN by both uFAST and manual pressing (Figure 4g).

3. Conclusion

In the last decade, the rapid development of unmanned aerial vehicles (UAVs) has realized the remarkably effective transport of medicines and emergency equipment due to their capability of spatially unrestricted, terrain-independent, and rapid arrival at targeted locations, greatly improving the survival rate of emergency patients.^[17] Besides the rapid transport of emergency medicine, a timely medication administration is also indispensable for preserving life. Nonetheless, the current medical UAVs still require emergency patients to administer drugs on their own or other people around them to help, which is not feasible in many situations. Therefore, there is an urgent need to develop a UAV-based system that can not only identify the position of patients and reach them immediately but also achieve autonomous drug administration to relieve symptoms.

We have developed a UAV-assisted autonomous drug delivery system for first aid. Our uFAST consists of the UAV, the CTMA, and the MN patch containing emergency therapeutics. Among them, the UAV could complete the reception of the emergency signal, generating trajectory to the target location, obstacle avoidance, and target recognition; the CTMA enables autonomous drug delivery to provide first aid without additional assistant; the MN patch offers a fast-acting and smart drug delivery for the emergency patient. Both simulation and real-world experiments indicated that CTMA could

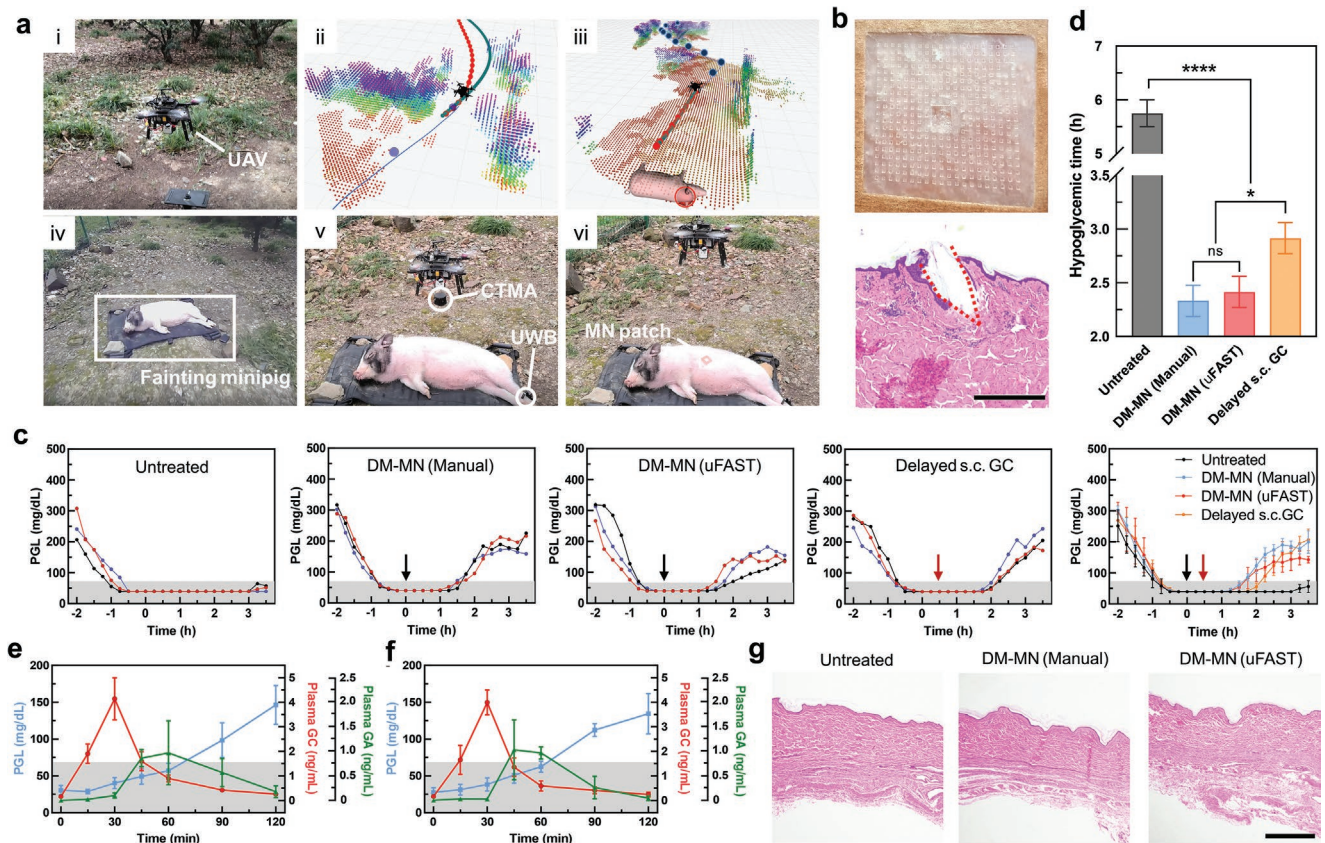


Figure 4. In vivo performance of the DM-MNs-integrated uFAST in an insulin-overdosing hypoglycemic diabetic minipig model. a) The working process of the DM-MN integrated uFAST in the minipig model. a-i) Autonomous take-off once the alert signal is received. a-ii) Automatic trajectory planning. Red track: optimized trajectory; Green track: global trajectory; Blue track: flight trajectory. Blue point: UWB sampling points. a-iii) Re-location. Blue point: UWB sampling points; Red point: corrected localization of minipig (the patient model). a-iv) Identification. a-v) Release of the CTMA. a-vi) Administration of the DM-MN patch toward the minipig skin. b) Top: photograph of DM-MN patch applied to the skin of the minipig by uFAST in (a), bottom: H&E-stained section of minipig skin penetrated by the DM-MN patch. Scale bar: 300 μ m. c) Plasma glucose levels (PGLs) in insulin-overdosing hypoglycemic diabetic minipigs ($n = 3$) without treatment or with treatments by different methods, including the DM-MN patches administered manually or by uFAST as well as subcutaneous GC injection delayed by 30 min. Patch size: 2 cm \times 2 cm. Insulin dose: 0.035 mg kg $^{-1}$. GC dose in DM-MNs: 1 mg. GA dose in DM-MNs: 3 mg. GC dose in injection: 1 mg. Black arrow, the time point of the DM-MNs administration. Red arrow, the time point of subcutaneous injection of GC. Gray area, PGLs below 70 mg dL $^{-1}$ (hypoglycemic range). d) Duration of hypoglycemia in minipigs ($n = 3$) received different treatments. e,f) PGLs and plasma concentrations of GC and GA in minipigs ($n = 3$) treated with the DM-MN patches manually (e) or by uFAST (f). g) H&E-stained skin sections of minipig skin pre- and post-treatment of DM-MNs. Scale bar: 1 mm. In (c-f), data are presented as mean \pm s.d. Statistical significance was determined by a two-tailed Student's t test. * $P < 0.05$ and *** $P < 0.0001$.

provide a uniform and sufficiently powerful force for the microneedle to be firmly inserted into the skin. Moreover, the MN patch with dual modes could not only offer a basal dose of the emergency drug at the first time but also support with a subsequent glucose-dependent dose to prevent the potential side effect of overdosing. In vivo studies confirmed that the uFAST successfully implemented autonomous first aid in a hypoglycemic minipig model, which effectively prevented the continuous decrease in blood glucose and promoted its rise to the normal range.

Furthermore, in order to improve the insertion rate of the MNs into the uneven skin, the flexible materials could be integrated at the bottom of CTMA, ensuring that CTMA can well fit the skin during the administration. In addition, wearable monitoring devices such as smart watches that can monitor physiological signals including blood pressure and heart rate, can be further paired with the uFAST.^[18] Once a dan-

gerous signal is identified by the wearable monitoring device, it could transmit the alert and position information to initiate the uFAST for first aid. Considering the impact of environment and positioning accuracy, several advanced detection or analysis regions could also be further combined with the uFAST. For example, the radar-based system (OUSTER OS0) and thermal images could be applied for detection in difficult weather conditions.^[14,19] The OpenPose system and Instance Mask Projection system could integrate for detecting real-time pose and delivering drugs to the targeted area (e.g., bare skin) to enhance the accuracy.^[20] Meanwhile, other formulations and administration approaches of drugs, such as transdermal creams and aerosols, even new delivery devices^[21] can be integrated with the uFAST to extend this platform of UAV-mediated drug delivery for emergency treatment of other sudden diseases and dangerous occasions associated with fires.

4. Experimental Section

Materials: All of the non-standard parts of CTMA were processed by nylon 3D printing made by WeNext. The UWB sensors (LinkTrack PS-B and LinkTrck PTag) were purchased from Noooploop. The USB camera (KS2A543) was purchased from Kingcent. The servo motor (HT-S-2806) was purchased from Haitai Electromechanical. The steering motor (LX-15D) was purchased from Hiwonder. All chemicals were purchased from Aladdin unless otherwise specified and used as received. Glucagon analog (sequence: HSQGTFTSDYSKYLDSSRRAQDFVQWLMNTRR) was ordered from GL Biochem Ltd. (Shanghai, China). Human glucagon (GC) was purchased from Bidet Pharmaceuticals (Catalog No. BD132093). Coomassie (Bradford) Protein Assay Kit was purchased from Thermo Fisher Scientific (Catalog No. 23200). Norland Optical Adhesive 86H was purchased from Edmund Optics (Catalog No. 12-848). Glucagon human enzyme-linked immunosorbent assay (ELISA) kit was purchased from Thermo Fisher Scientific (Catalog No. EHGCG). (4-((2-acrylamidoethyl) carbamoyl)-3-fluorophenyl) boronic acid was purchased from AmBeed (Catalog No. A1194179). Streptozocin (STZ) was purchased from MACKLIN (Catalog No. S817944).

Autonomous UAV-Mediated Microneedle Delivery in the Forest: The FAST 330 UAV was utilized to integrate the autonomous medicine delivery system in this study. The quadrotor was equipped with an Nvidia Xavier NX for onboard computing, an Intel RealSense D435 stereo camera pair for imagery and depth sensing, and a PX4 autopilot for stabilizing the drone and feeding inertial measurement unit data. A manual estimate was applied as a danger signal (based on CGMS) to send the initial approximate position information of the patient (minipig). To estimate and correct the localization of the patient, the relative distance between uFAST and the patient was measured by using the onboard UWB sensor. To further smooth the position of the patient based on the detection of YOLOv5, a lowpass filter was applied. Once the uFAST hovered stably at the expected position, the CTMA was released.

CTMA Characterizations: To keep the consistency of the experiment conditions, the CTMA was released from the release device, and the device without spring was made by fixing the CTMA with its slideable base with glue. The impulse measuring test was performed using a high-speed camera (PHANTOM Miro C210) to record images at the rate of 4000 fps (Figure S4, Supporting Information), whose interval time Δt was 250 μs . The initial velocity v_0 was determined by the RH h calculated as $v_0 = \sqrt{2gh}$. The initial and the final frame numbers were manually determined with the interval of $n = 40$. The initial frame referred to a frame at which the base of the CTMA first left the skin. The displacement Δx was defined as the distance between the center of gravity of the CTMA at the selected frame numbers. The generated impulse was calculated as: $I = m\Delta v$, where $\Delta v = v_1 - v_0 = (\Delta x/n\Delta t) - (\sqrt{2gh}(g/l|g|))$.

Positioning Accuracy of CTMA: In the *in vitro* experiment, to precisely locate the MN patch position after using the CTMA, 40% gelatin was chosen as the skin model for the MNs position recording. The MN patch was fixed on the CTMA. After releasing the CTMA at different heights, the MN patch lodged into the gelatin to leave an imprint. Photographs of the gelatin with the MNs imprint were subsequently taken and the location of the MN patch position was depicted by CorelDraw for further analysis. In the *in vivo* experiment, the CTMA was assembled on the UAV. The CTMA was released when the UAV reached above the minipig by identifying the minipig. The release process of the CTMA and the position of the MN patch were recorded by the camera fixed on the UAV.

Blood-Glucose-Raising Effect of GA: GA and GC were dissolved in 0.01 M HCl solution and configured into 1 mg mL⁻¹ solution, respectively. The initial blood glucose of each mouse was measured by a glucometer (Accu-Chek Aviva). The GC and GA were injected subcutaneously into healthy C57BL/6 mice at a dose of 15 mg kg⁻¹, followed by a measurement of blood glucose level after 15 min of injection. The animal study protocol was approved by the Institutional Animal Care and Use Committee at Zhejiang University.

Fabrication of DM-MN Patch: The DM-MN patch was prepared by press alignment and twice polymerization under ultraviolet irradiation. In brief, to prepare the DM-MN, a total of two microneedle molds were

used: a 400 × 400 μm base and 500 μm height pyramid mold and a 400 × 400 μm base and 400 μm height square prism mold, respectively. The needles in both molds were arranged in a 20 × 20 array with a spacing of 400 μm . The glucose-responsive part of the DM-MN was first prepared. The ethylene glycol dimethacrylate (EGDMA) (0.5 wt%) as the crosslinker and 2-hydroxy-4'-(2-hydroxyethoxy)-2-methylpropiophenone (Irgacure 2959) (1.5 wt%) as the photoinitiator were dissolved in *N*-vinylpyrrolidone (NVP) solution, followed by the addition of (4-((2-acrylamidoethyl) carbamoyl)-3-fluorophenyl) boronic acid (3FPBA) and 2-(dimethylamino) ethyl acrylate (DMAEA) in a molar ratio of 1:0.8 to the mixture. The mixture then placed under ultrasound until completely dissolved. Afterward, the GA (12 wt%) was dispersed in the prepared monomer, mixed thoroughly under ultrasonication, and the solution was directly deposited by pipette onto the surface of the square prism molds. Then, the molds were placed under vacuum for 20 min to allow the solution to fill the mold cavities. After removing the excess solution, the mold on an ice bath was placed under a UV curing lamp for 5 min of photopolymerization (135 mW cm⁻², 365 nm). The UV curable substrate (NOA 86H) was then added dropwise to the mold and cured under a UV lamp for 5 min to obtain the glucose-responsive module of DM-MN. The immediate release module of the DM-MN was subsequently prepared in a similar manner. The mixture of the immediate release part contained only NVP, Irgacure 2959 (1.5 wt%), and GC (10 wt%), and was deposited by pipette onto the surface of the pyramid mold. To integrate the immediate release module and glucose-responsive release module, the glucose-responsive release part was aligned and inserted into the pyramid microneedle mold filled with the immediate release module of the monomer solution under a stereomicroscope, and the mold was placed on an ice bath under a UV curing lamp for 5 min for photopolymerization (135 mW cm⁻², 365 nm). The resulting patch was carefully separated from the mold and stored in the vacuum desiccator for further studies.

Microneedle Characterizations: The fluorescence images of the DM-MN were observed using a fluorescence microscope (Nikon). Nova Nano 450 field-emission scanning electron microscope (SEM) was applied to characterize the DM-MN patch. The DM-MN patch was sputtered with a gold/palladium target for 30 s prior to imaging. The mechanical strength of the microneedle was measured by pressing the microneedle against a stainless-steel plate. The initial gauge between the microneedle tip and the stainless-steel plate was set at 1.00 mm and the load cell capacity was 10.00 N. The top stainless-steel plate was moved toward the microneedle at a speed of 0.1 mm s⁻¹. The failure force of the microneedles was recorded when the needles began to buckle.

MALDI-TOF Spectra: GC was extracted from the immediate release part of the prepared DM-MN patch in PBS solution for 5 min, and GA was extracted from the glucose-responsive release part of DM-MN in 0.01 M HCl at 4 °C for 24 h. The spectra of the released GC, GC, the released GA, and GA were detected using an Ultraflextreme MALDI-TOF/TOF system.

In Vitro Release Studies: To assess the immediate release of GC and glucose-responsive release of GA, the immediate release and responsive-release modules of the DM-MN patch were placed in 1 mL of PBS solution (pH 7.4), respectively, and incubated at 37 °C with gentle shaking (400 rpm) at different glucose concentrations (50, 100, and 200 mg dL⁻¹). At predetermined time points, 10 μL of supernatant was collected into 96-well plates and released GC or GA was quantified using the Coomassie (Bradford) protein assay (Thermo Fisher Scientific). Absorbance was detected at 595 nm on the Synergy H1 microplate reader (BioTek) and concentrations were calculated using GC (8–500 μg mL⁻¹) or GA (8–500 μg mL⁻¹) standard curves. The release patterns of GC and GA integrated in the DM-MN patch were performed in the same way, where the GC and GA were labeled with FITC and rhodamine B, respectively. The release of GC and GA was detected by a fluorometric method (GC: excitation wavelength: 490 nm, emission wavelength: 520 nm; GA: excitation wavelength: 540 nm, emission wavelength: 593 nm), and the concentration of FITC-labeled GC (0–500 μg mL⁻¹) and rhodamine-B-labeled GA (0–500 μg mL⁻¹) standard curve were used to calculate the concentration.

Cytotoxicity of the DM-MN: The immediate release part of DM-MN was re-dissolved in DMEM medium and added to B16F10 cells for 24 h, and cell viability was detected using the CCK-8 kit.

In Vivo Studies Using an Insulin-Overdosing Hypoglycemic Diabetic Minipig Model: The animal study protocol was approved by the Institutional Animal Care and Use Committee at Zhejiang University. Three male Bama minipigs were used. Insulin-deficient diabetes was induced in minipigs by intravenous administration of STZ (150 mg kg⁻¹). STZ was dissolved in freshly prepared sodium citrate–disodium citrate buffer (pH 4.5) under light-protected conditions at a final intravenous concentration of 75 mg mL⁻¹ and was administered intravenously within 10 min. The successful establishment of an insulin-deficient diabetes minipig model was confirmed by monitoring glucose levels with a continuous glucose monitor system (CGMS, FreeStyle Libre, Abbott) affixed to the inner hind limbs of the minipig after 7 days of STZ injection. Diabetic minipigs were treated once daily with glargin insulin (0.3–0.8 U kg⁻¹; Lantus; Sanofi) for glycemic control. Daily treatment was stopped 36 h before the experiment. All minipigs (25–30 kg) were fasted overnight before the experiment and an overdose of insulin (0.035 mg kg⁻¹) was injected subcutaneously on the following day. After blood glucose level was at a hypoglycemic level (<70 mg dL⁻¹), DM-MN was applied to the flanks of the minipigs by using different methods, and the doses of GC and GA in each patch were 1.0 and 3.0 mg, respectively. The minipigs were under anesthesia during the application of the patch. Before applying DM-MN, the hair on the lateral side of the minipig was shaved, and the microneedle was inserted into the shaved skin by hand pressing or by uFAST. To secure the patch on the skin surface, a 3M Tegaderm transparent film dressing was used to cover the patch. Before applying DM-MN through the uFAST, DM-MN was attached to a 3 M film dressing and secured to the CTMA. Blood glucose changes were continuously monitored by CGMS during the experiment. To verify that the elevated glucose and drug release were correlated, the concentrations of GC and GA in plasma were measured by ELISA and fluorometric methods, respectively. After applying the DM-MN patch in different ways, blood was collected from the anterior vena cava at the indicated time points and blood glucose levels were measured by using a glucometer (Accu-Chek Aviva glucometer, Roche Diabetes Care Inc.). The plasma was then extracted from blood by centrifugation (3000 rpm, 20 min) and stored at –20 °C until it was assayed.

H&E Staining: DM-MN patches were applied to the shaved skin of minipigs using different methods (manually and by uFAST), and 1 day after removal of DM-MN, the skin was obtained from the treatment site, fixed in 4% formaldehyde for 24 h, and sectioned and stained with H&E.

Statistical Analysis: All the results are presented as mean ± s.d. Statistical analysis was performed using a two-tailed Student's t-test. The differences between experimental groups and control groups were considered statistically significant at *P*<0.05.

Supporting Information

Supporting Information is available from the Wiley Online Library or from the author.

Acknowledgements

T.S. and R.J. contributed equally to this work. The authors acknowledge Deyue Xu (Laboratory Animal Center, Zhejiang University), Mengke Zhang, Liua Pei, Chengzhang Gong, Haoxiong Xu, and Kunyi Zhang for helping in animal field experiments. The authors appreciate Chao Sun (Analysis Center of Agrobiology and Environmental Sciences, Zhejiang University) for the help of MALDI mass analysis and Guizhen Zhu, Dandan Song (Cryo-EM center, Zhejiang University) for help in processing of samples for scanning electron microscopy. This work

was supported by the grants from the National Key R&D Program of China (2021YFA0909900) to Z.G., National Science Foundation of China (62173293) to R.X., Zhejiang Provincial Natural Science Foundation of China (LD22E050007), the Fundamental Research Funds for the Zhejiang Provincial Universities (2021XZX021) to H.L., and the grants from the Startup Package of Zhejiang University to and Y.Z., H.L., J.Y., and Z.G.

Conflict of Interest

Z.G., J.Y., H.L., Y.Z., F.G., T.S., and R.J. have applied for patents related to this study. Z.G. is the co-founder of Zenomics Inc., Zencapsule Inc., Lizen Inc., Wskin Inc., and ZCapsule Inc. Z.G. and Y.Z. are the co-founders of μZen Pharma Co., Ltd., and the other authors declare no conflict of interest.

Data Availability Statement

The data that support the findings of this study are available from the corresponding author upon reasonable request.

Keywords

drug delivery, first aid, microneedles, unmanned aerial vehicles

Received: September 20, 2022

Revised: October 31, 2022

Published online: January 29, 2023

- [1] a) P. Deedwania, *J. Am. Coll. Cardiol.* **2018**, *72*, 1787; b) E. M. Singletary, D. A. Zideman, J. C. Bendall, D. C. Berry, V. Borra, J. N. Carlson, P. Cassan, W. T. Chang, N. P. Charlton, T. Djavari, M. J. Douma, J. L. Epstein, N. A. Hood, D. S. Markenson, D. Meyran, A. M. Orkin, T. Sakamoto, J. M. Swain, J. A. Woodin, F. A. S. Collaborators, *Circulation* **2020**, *142*, S284; c) C. Andersson, R. S. Vasan, *Nat. Rev. Cardiol.* **2018**, *15*, 230.
- [2] a) G. De Luca, H. Suryapranata, J. P. Ottavanger, E. M. Antman, *Circulation* **2004**, *109*, 1223; b) J. Emberson, K. R. Lees, P. Lyden, L. Blackwell, G. Albers, E. Bluhmki, T. Brott, G. Cohen, S. Davis, G. Donnan, J. Grotta, G. Howard, M. Kaste, M. Koga, R. von Kummer, M. Lansberg, R. I. Lindley, G. Murray, J. M. Olivot, M. Parsons, B. Tilley, D. Toni, K. Toyoda, N. Wahlgren, J. Wardlaw, W. Whiteley, G. J. del Zoppo, C. Baigent, P. Sandercock, W. Hacke, et al., *Lancet* **2014**, *384*, 1929; c) C. P. Cannon, C. M. Gibson, C. T. Lambrew, D. A. Shoultz, D. Levy, W. J. French, J. M. Gore, W. D. Weaver, W. J. Rogers, A. J. Tiefenbrunn, *JAMA, J. Am. Med. Assoc.* **2000**, *283*, 2941.
- [3] a) A. B. Jena, C. Mann, L. N. Wedlund, A. Olenski, *N. Engl. J. Med.* **2017**, *376*, 1441; b) Z. Kmietowicz, *BMJ* **2017**, *358*, j4339; c) J. S. Baekgaard, S. Viereck, T. P. Moller, A. K. Ersboll, F. Lippert, F. Folke, *Circulation* **2017**, *136*, 954.
- [4] C. Vergari, J. C. Mansfield, D. Chan, A. Clarke, J. R. Meakin, P. C. Winlove, *Acta Biomater.* **2017**, *63*, 274.
- [5] a) E. Kochba, Y. Levin, I. Raz, A. Cahn, *Diabetes Technol. Ther.* **2016**, *18*, 525; b) Y. Ye, J. Yu, D. Wen, A. R. Kahkoska, Z. Gu, *Adv. Drug Delivery Rev.* **2018**, *127*, 106; c) S. P. Sullivan, D. G. Koutsonanos, M. D. Martin, J. W. Lee, V. Zarnitsyn, S. O. Choi, N. Murthy, R. W. Compans, I. Skountzou, M. R. Prausnitz, *Nat. Med.* **2010**, *16*, 915; d) A. Abramson, E. Caffarel-Salvador, V. Soares, D. Minahan, R. Y. Tian, X. Y. Lu, D. Dellal, Y. Gao, S. Kim, J. Wainer, J. Collins, S. Tamang, A. Hayward, T. Yoshitake,

- H. C. Lee, J. Fujimoto, J. Fels, M. R. Frederiksen, U. Rahbek, N. Roxhed, R. Langer, G. Traverso, *Nat. Med.* **2019**, *25*, 1512; e) M. R. Prausnitz, R. Langer, *Nat. Biotechnol.* **2008**, *26*, 1261; f) W. Li, R. N. Terry, J. Tang, M. H. R. Feng, S. P. Schwendeman, M. R. Prausnitz, *Nat. Biomed. Eng.* **2019**, *3*, 220; g) J. C. Yu, Y. Q. Zhang, Y. Q. Ye, R. DiSanto, W. J. Sun, D. Ranson, F. S. Ligler, J. B. Buse, Z. Gu, *Proc. Natl. Acad. Sci. U. S. A.* **2015**, *112*, 8260; h) J. C. Yu, J. Q. Wang, Y. Q. Zhang, G. J. Chen, W. W. Mao, Y. Q. Ye, A. R. Kahkoska, J. B. Buse, R. Langer, Z. Gu, *Nat. Biomed. Eng.* **2020**, *4*, 499; i) P. C. DeMuth, Y. J. Min, B. Huang, J. A. Kramer, A. D. Miller, D. H. Barouch, P. T. Hammond, D. J. Irvine, *Nat. Mater.* **2013**, *12*, 367; j) K. Lee, M. J. Goudie, P. Tebon, W. J. Sun, Z. M. Luo, J. Lee, S. M. Zhang, K. Fetah, H. J. Kim, Y. M. Xue, M. A. Darabi, S. Ahadian, E. Sarikhani, W. Ryu, Z. Gu, P. S. Weiss, M. R. Dokmeci, N. Ashammakhi, A. Khademhosseini, *Adv. Drug Delivery Rev.* **2020**, *165–166*, 41.
- [6] K. V. Allen, B. M. Frier, *Endocr. Pract.* **2003**, *9*, 530.
- [7] a) J. Geddes, J. E. Schopman, N. N. Zammit, B. M. Frier, *Diabetic Med.* **2008**, *25*, 501; b) E. W. M. T. ter Braak, A. M. M. F. Appelman, M. F. van de Laak, R. P. Stolk, T. W. van Haeften, D. W. Erkelens, *Diabetes Care* **2000**, *23*, 1467.
- [8] T. A. Hitt, J. Smith, E. L. Forth, P. Garren, D. Olivos-Stewart, M. De la Vega, F. Stuart, C. P. Hawkes, S. M. Willi, J. Gettings, *Diabetes* **2020**, *69*, 1292.
- [9] S. Diridollou, F. Patat, F. Gens, L. Vaillant, D. Black, J. M. Lagarde, Y. Gall, M. Berson, *Skin Res. Technol.* **2000**, *6*, 214.
- [10] M. C. Jaklevic, *JAMA, J. Am. Med. Assoc.* **2021**, *325*, 613.
- [11] a) S. S. Steiner, M. Li, R. Hauser, R. Pohl, J. *Diabetes Sci. Technol.* **2010**, *4*, 1332; b) Z. Wang, J. Wang, H. Li, J. Yu, G. Chen, A. R. Kahkoska, V. Wu, Y. Zeng, D. Wen, J. R. Miedema, J. B. Buse, Z. Gu, *Proc. Natl. Acad. Sci. U. S. A.* **2020**, *117*, 29512.
- [12] A. Surnmerfield, F. Meurens, M. E. Ricklin, *Mol. Immunol.* **2015**, *66*, 14.
- [13] T. Qin, P. L. Li, S. J. Shen, *IEEE Trans. Rob.* **2018**, *34*, 1004.
- [14] Z. Wang, X. Zhou, C. Xu, F. Gao, *IEEE Trans. Rob.* **2022**, *38*, 3259.
- [15] X. Zhou, Z. P. Wang, H. K. Ye, C. Xu, F. Gao, *IEEE Rob. Autom. Lett.* **2021**, *6*, 478.
- [16] D. P. Zaharieva, K. Turksoy, S. M. McGaugh, R. Pooni, T. Vienneau, T. Ly, M. C. Riddell, *Diabetes Technol. Ther.* **2019**, *21*, 313.
- [17] a) D. C. Schedl, I. Kurmi, O. Bimber, *Sci. Rob.* **2021**, *6*, eabg1188.
b) A. Claesson, A. Backman, M. Ringh, L. Svensson, P. Nordberg, T. Djärv, J. Hollenberg, *JAMA, J. Am. Med. Assoc.* **2017**, *317*, 2332;
c) S. Schierbeck, J. Hollenberg, A. Nord, L. Svensson, P. Nordberg, M. Ringh, S. Forsberg, P. Lundgren, C. Axelsson, A. Claesson, *Eur. Heart J.* **2021**, *42*, 656; d) M. P. Nisingizwe, P. Ndishimye, K. Swaibu, L. Nshimiyimana, P. Karame, V. Dushimiyimana, J. P. Musabyimana, C. Musanabaganwa, S. Nsanizimana, M. R. Law, *Lancet Global Health* **2022**, *10*, e564.
- [18] M. A. C. Gil, *Eur. Heart J.* **2021**, *42*, 3046.
- [19] M. Krišto, M. Ivasic-Kos, M. Pobar, *IEEE Access* **2020**, *8*, 125459.
- [20] a) Z. Cao, T. Simon, S.-E. Wei, Y. Sheikh, in *2017 IEEE Conf. on Computer Vision and Pattern Recognition (CVPR)*, IEEE, Piscataway, NJ, USA **2017**, pp. 1302–1310. b) C. Fu, T. Berg, A. Berg, in *2019 IEEE/CVF Int. Conf. on Computer Vision (ICCV)*, IEEE, Piscataway, NJ, USA **2019**, pp. 5177–5186.
- [21] A. Abramson, E. Caffarel-Salvador, M. Khang, D. Dellal, D. Silverstein, Y. Gao, M. R. Frederiksen, A. Vegge, F. Hubalek, J. J. Water, A. V. Friderichsen, J. Fels, R. K. Kirk, C. Cleveland, J. Collins, S. Tamang, A. Hayward, T. Landh, S. T. Buckley, N. Roxhed, U. Rahbek, R. Langer, G. Traverso, *Science* **2019**, *363*, 611.